CrossMark

RESEARCH ARTICLE

Enhanced Scalar Concentrations and Fluxes in the Lee of Forest Patches: A Large-Eddy Simulation Study

Farah Kanani-Sühring[1] · **Siegfried Raasch**[1]

Abstract By means of large-eddy simulation, we investigate the transport of a passive scalar in the lee of forest patches under neutral atmospheric conditions in flat terrain. We found a pronounced local enhancement of scalar concentration and scalar flux in the lee zone of the forest, while further downstream above the unforested surface, the scalar transport adjusted to an equilibrium with the underlying surface conditions. By means of a term-by-term analysis of the scalar transport equation, we determined the local accumulation of the scalar to be caused by the convergence of: (1) mean and turbulent streamwise transport, (2) mean vertical transport. However, the relative importance of each transport mechanism for the accumulation process was found to depend strongly on forest density. Based on systematic parameter changes, we found concentrations to significantly increase with increasing forest density and with decreasing wind speed, while fluxes were invariant to wind speed and showed a similar relation to forest density as for the concentrations. Despite the scalar sources—ground and/or canopy sources—a local flux enhancement was present in the lee zone. Finally, we provide a first step towards localizing enhanced concentrations and fluxes at micrometeorological sites.

Keywords Enhanced scalar fluxes · Forest-edge flow · Large-eddy simulation · Lee recirculation · Scalar accumulation

1 Introduction

The transport of scalars such as temperature, humidity and trace gases (e.g. CO_2) is highly complex in fragmented forested landscapes, hence, it is subject to ongoing studies mostly of a numerical nature due to the difficulty in obtaining three-dimensional views of such processes in the field. Previous studies (Klaassen et al. 2002; Sogachev et al. 2008; Ross and Baker 2013;

✉ Farah Kanani-Sühring
kanani@muk.uni-hannover.de

[1] Institut für Meteorologie und Klimatologie, Leibniz Universität Hannover, Herrenhäuser Str. 2, 30419 Hannover, Germany

Kanani-Sühring and Raasch 2015) have shown that mean and turbulent transport processes are markedly modified near clearing-to-forest transitions (windward forest edge), as compared to further upstream or downstream, leading to locally enhanced scalar concentrations and scalar fluxes. This is attributed to flow convergence due to the abrupt change of the mechanic and thermodynamic surface properties at the transition. The mentioned studies mainly focused on flows over windward forest edges in flat terrain, while Ross and Baker (2013) were one of the first to model scalar transport near windward and leeward forest edges in hilly terrain. With the scalar source being the forest volume, they found that a local scalar accumulation can be observed at different locations within the forest patch, depending on the position of the patch with respect to the hill ridge. Ross and Harman (2015) examined the effect of the scalar source distribution on the spatial variability of concentrations and fluxes, finding significant differences between ground/sub-canopy sources and canopy sources. All of this questions the spatial representativity of local measurements under such conditions. Understanding scalar transport in complex terrain is crucial for the design and interpretation of in situ measurements, as well as for evaluating and improving parametrizations of scalar transport in numerical weather prediction and climate models. Our study focuses on how scalar transport behaves in the lee of forests in flat terrain, for various forest densities, and under different meteorological and scalar-source conditions.

Flows in the lee of permeable obstacles, such as forest patches (Bergen 1975; Miller et al. 1991; Cassiani et al. 2008; Detto et al. 2008; Frank and Ruck 2008; Belcher et al. 2012; Queck et al. 2015), exhibit distinct flow patterns such as flow separation, recirculation and re-attachment. Similar patterns are observed in the lee of hills (Raupach et al. 1992; Finnigan and Belcher 2004; Katul et al. 2006; Poggi and Katul 2007; Ross 2008, 2011), single buildings (e.g. Letzel et al. 2008, 2012) or sharp steps (e.g. Armaly et al. 1983; Kostas et al. 2002; Markfort et al. 2014), and within street canyons (e.g. Chan et al. 2002; Cai et al. 2008; Fontan et al. 2013). For example, in the lee of crosswind-elongated hills or sharp steps, flows tend to recirculate due to pressure redistribution, before re-attaching to the surface behind the obstacle. This was found mostly from laboratory studies (e.g. Chan et al. 2002; Poggi and Katul 2007; Fontan et al. 2013; Markfort et al. 2014) and numerical simulations (e.g. Raupach et al. 1992; Katul et al. 2006; Frank and Ruck 2008; Ross 2008, 2011). In the past few decades, special attention has been addressed to the flow across abrupt solid surface steps, termed backward-facing-step (BFS) flows, extensively studied in the wind tunnel and in numerical simulations using Reynolds-averaged Navier–Stokes (RANS) or large-eddy simulation (LES) models. The purpose of such BFS-flow studies was mostly directed towards urban applications, e.g. to the investigation of street-canyon ventilation or pollutant dispersion.

Flows in the lee of permeable steps also show features of BFS flow (Cassiani et al. 2008; Detto et al. 2008), but cannot be described as a pure BFS flow since a fraction of the flow originates from the forest interior, referred to as the exit flow (Cassiani et al. 2008; Detto et al. 2008). Using LES, Cassiani et al. (2008) found that both BFS and exit flows form an intermittent composition in the lee of forests. This was also reported by Detto et al. (2008) based on field measurements near a leeward forest edge, where they identified an intermittent rotor formation in sonic anemometer data. Such alternating rotor- and through-flow periods were already identified by Bergen (1975), based on a smoke-release experiment in a forest gap. Cassiani et al. (2008) further concluded that the relative contributions of BFS and exit flows strongly depend on forest density, with a more frequent occurrence of BFS events in the lee of denser forests.

In heterogeneous flow regimes, not only are the flow dynamics locally perturbed, but the transport of scalars between land surface, vegetation and atmosphere is too. In a wind-

tunnel experiment on the flow across a forested hill, Poggi and Katul (2007) detected a local accumulation of fluorescent dye within the rotor region on the lee side of the hill. Similar results were found by Katul et al. (2006) and Ross (2011) from RANS and LES with similar set-ups; they reported large streamwise variations of the tracer concentration across the hill, with maximum concentrations near the separation point on the lee side, accompanied by enhanced tracer fluxes. Also in the lee of abrupt steps, local tracer accumulations have been detected in numerical simulations (e.g. Chan et al. 2002) and flume experiments (e.g. Fontan et al. 2013). So far, only a few studies have focused on the flow in the lee of forest patches (Cassiani et al. 2008; Detto et al. 2008; Markfort et al. 2014), and even less attention has been paid to the scalar transport in such flow regimes. Since a forest-lee flow shows similarities with the flow behind solid obstacles, the scalar transport and the scalar distribution supposedly share some features in both regimes. However, due to the intermittence of BFS-flow and exit-flow events in a forest-edge flow (permeable step), as compared to a pure BFS flow (solid step), the scalar transport might strongly depend on the forest morphology.

The scope of the present LES study is to examine, for the first time in detail, the transport and the spatial distribution of a passive scalar in the lee of a spanwise elongated forest patch. Due to the yet scarce understanding, an idealized set-up is purposely selected, treating neutrally-stratified flows in flat terrain across a periodic forest–clearing–forest configuration. We analyze how scalar concentrations and fluxes react under a range of conditions, e.g. for different forest densities and mean wind speeds, as well as with different scalar sources. One of the main questions is to what extent the background conditions and the permeability of the forest modify the scalar transport in the forest lee. Further, the present study aims at identifying the resulting implications for the design and interpretation of micrometeorological measurements close to leeward forest edges.

Section 2 briefly describes the applied LES model and the simulation designs used. Simulation results are discussed in Sect. 3, starting with the general flow features in the lee of the forest patch (Sect. 3.1), followed by a visualization of the scalar accumulation and an analysis of the scalar transport mechanisms (Sect. 3.2). Section 3.3 deals with the behaviour of the spatial distribution of scalar concentration and scalar flux under the different simulated conditions. In Sect. 3.4, we introduce a possible approach for planning and interpreting micrometeorological measurements in the lee of forest patches. The main results are summarized in Sect. 4.

2 Methods

The investigation of the scalar transport in the lee of forests, as a follow-up study to that of Kanani-Sühring and Raasch (2015) on the scalar transport inside and above a forest patch, is based on LES data for the same idealized simulations. The parallelized LES model PALM (Raasch and Schröter 2001), at version 3.8 revision 874[1], was applied with its embedded canopy model, in order to explicitly resolve the turbulent transport of a passive scalar, and to analyze its disturbance by a forest edge. Fundamental equations for the simulation of an atmospheric flow in PALM, the formulation of the embedded canopy model, applied numerics and boundary conditions, as well as a detailed description and justification of the

---

[1] The code can be accessed under http://palm.muk.uni-hannover.de/browser?rev=874. A documentation of the most recent PALM release 4.0, with a detailed description of PALM's canopy model, is given by Maronga et al. (2015).
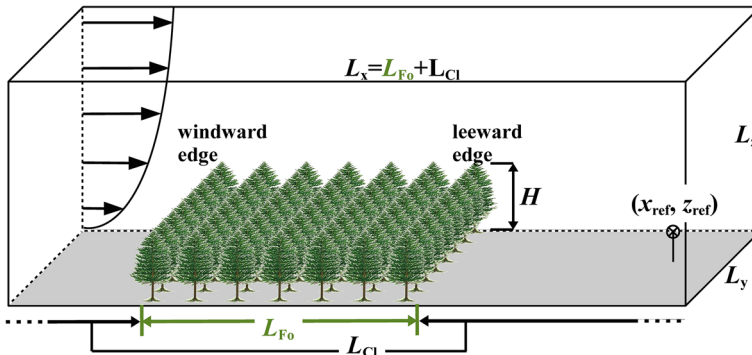
Fig. 1 Sketch of the LES model domain. L_x, L_y, L_z are domain length, width and height, respectively. The forest extends over a length of $L_{Fo} = 33H$ in the x-direction and over the total domain width L_y. The forest height is $H = 30$ m. The clearing length $L_{Cl} = 44H$ describes the total length of the unforested part of the domain. The flow (*arrows*) is directed perpendicular to the forest edge. The *grey* surface illustrates the homogeneous scalar source. ($x_{ref} = 33H$, $z_{ref} = 0.35H$) describe coordinates of the reference position, where e.g. reference wind speed u_{ref} is defined

simulation set-ups and the case studies, can be found in Kanani-Sühring and Raasch (2015). Nevertheless, part of the set-up information is briefly summarized below.

The LES model domain, as illustrated in Fig. 1, had a streamwise (x), spanwise (y) and vertical (z) extent of $L_x = 77H$, $L_y = 38H$ and $L_z = 13H$, respectively, with forest height $H = 30$ m. A uniform grid spacing of 3 m was used in each spatial direction. The forest patch covered the length $L_{Fo} = 33H$ of the domain surface in the x-direction, and the entire y-direction, where the total length of the clearing (unforested part of the domain) resulted in $L_{Cl} = L_x - L_{Fo} = 44H$. Lateral boundaries were cyclic, resulting in a periodic repetition of forest and clearing patches. The forest density was homogeneous in the horizontal directions, while the vertical distribution of the leaf area density $a(z)$ was heterogeneous, with the bulk of the leaf area concentrated in the crown space. Vertical profiles of $a(z)$ are presented in Fig. 2a for different leaf area indices [*LAI*: vertical integral of $a(z)$]. The canopy drag coefficient c_d, which appears as a constant in the PALM canopy model (see e.g. Kanani-Sühring and Raasch 2015), was set to a typical value for trees of 0.2 as in previous studies (e.g. Cassiani et al. 2008; Dupont and Brunet 2008). A purely shear-driven neutrally-stratified flow with omitted Coriolis force was simulated by prescribing a longitudinal pressure gradient $\partial p / \partial x$ (see Table 1), oriented perpendicular to the forest edge (u-velocity component). After the flow had reached a steady state, a passive scalar S was released with one of the following source configurations:

– Ground source: horizontally homogeneous (see grey-shaded surface in Fig. 1) at a constant rate of $Q_g = 0.2\ \mu g\,m^{-2}\,s^{-1}$,
– Canopy source: $Q_c = c_S\,a\,U\,(S(x, y, z) - S_l)$, with the scalar exchange coefficient $c_S = 0.0125$, leaf surface concentration $S_l = 20\ \mu g\,m^{-3}$, and $U = \sqrt{u^2 + v^2 + w^2}$ [the relation between ground and canopy source strength is equivalent to that used by Ross and Harman (2015)],
– Ground plus canopy source.

If not mentioned otherwise, presented results are from simulations with a source at the ground.

As listed in Table 1, eight simulations with different *LAI* values were performed (see Fig. 2a), at a given reference wind speed of $u_{ref} = 4.6$ m s^{-1}, and six simulations with
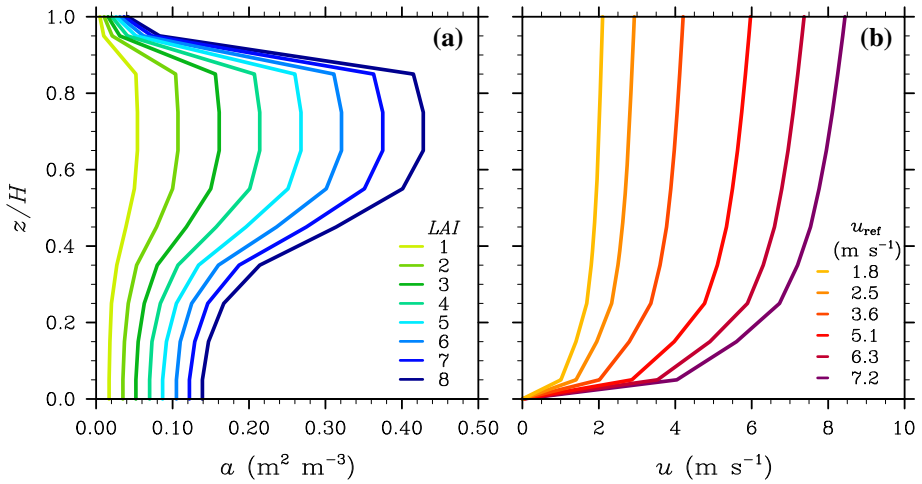
Fig. 2 Vertical profiles of **a** leaf area densities and **b** steady-state wind profiles of the mean flow (*u*-component) at position x_{ref}, used here as in Kanani-Sühring and Raasch (2015)

Table 1 Overview of the *LAI* values, longitudinal pressure gradients $\partial p/\partial x$ and reference velocities u_{ref} used here

LES run	*LAI*	$\partial p/\partial x$ (Pa m^{-1})	u_{ref} (m s^{-1})	Source
LAI1	1	−0.0017	4.6	Ground
LAI2	2	−0.0017	4.6	Ground
LAI3	3	−0.0017	4.6	Ground
LAI4	4	−0.0017	4.6	Ground
				Canopy
				Ground + canopy
LAI5	5	−0.0017	4.6	Ground
LAI6	6	−0.0017	4.6	Ground
LAI7	7	−0.0017	4.6	Ground
LAI8	8	−0.0017	4.6	Ground
UREF1	4	−0.00025	1.8	Ground
UREF2	4	−0.0005	2.5	Ground
UREF3	4	−0.001	3.6	Ground
UREF5	4	−0.002	5.1	Ground
UREF6	4	−0.003	6.3	Ground
UREF7	4	−0.004	7.2	Ground

different wind speeds (see Fig. 2b) at a constant $LAI = 4$. Reference wind speed u_{ref} equals the time- and *y*-averaged streamwise velocity component *u* at ($x_{ref} = 33H$, $z_{ref} = 0.35H$) above the clearing downstream of the leeward forest edge.

The scalar transport is analyzed by means of terms in the scalar transport equation, as previously described and applied by Kanani-Sühring and Raasch (2015), briefly summarized as,

$$\underbrace{\frac{\partial \langle S \rangle}{\partial t}}_{I} = -\frac{\partial \langle u_i \rangle \langle S \rangle}{\partial x_i} \qquad -\frac{\partial \langle u_i' S' \rangle}{\partial x_i} \qquad +\frac{\partial}{\partial x_i}\left\langle K_{\text{s}} \frac{\partial S}{\partial x_i}\right\rangle \; - \; Q_{\text{c}}$$

$$= \underbrace{-\frac{\partial \langle u \rangle \langle S \rangle}{\partial x}}_{IIa} \qquad \underbrace{-\frac{\partial \langle u' S' \rangle}{\partial x}}_{IIIa} \qquad \underbrace{+\frac{\partial}{\partial x}\left\langle K_{\text{s}} \frac{\partial S}{\partial x}\right\rangle}_{IVa}$$

$$\underbrace{-\frac{\partial \langle v \rangle \langle S \rangle}{\partial y}}_{IIb} \qquad \underbrace{-\frac{\partial \langle v' S' \rangle}{\partial y}}_{IIIb} \qquad \underbrace{+\frac{\partial}{\partial y}\left\langle K_{\text{s}} \frac{\partial S}{\partial y}\right\rangle}_{IVb}$$

$$\underbrace{-\frac{\partial \langle w \rangle \langle S \rangle}{\partial z}}_{IIc} \qquad \underbrace{-\frac{\partial \langle w' S' \rangle}{\partial z}}_{IIIc} \qquad \underbrace{+\frac{\partial}{\partial z}\left\langle K_{\text{s}} \frac{\partial S}{\partial z}\right\rangle}_{IVc} \; - \; Q_{\text{c}}, \qquad (1)$$

with velocity components $u_i \in \{u_1 = u, u_2 = v, u_3 = w\}$ and time t; K_{S} is the subgrid-scale diffusion coefficient of the scalar S. Angled brackets denote a line average parallel to the forest edge (y-direction), and a prime describes a fluctuation from this line average. Term I quantifies the local temporal change of S, resulting from the net transport of S by: the mean flow (II), resolved-scale turbulence (III) and subgrid-scale turbulence (IV), in the edge-perpendicular (a), edge-parallel (b) and vertical (c) direction. Q_{c} is the canopy source term. Terms (II-IV)b are zero by definition, owing to the averaging in the y-direction; nevertheless, net transports along y should on average be negligible since the mean flow is statistically homogeneous in this direction. A positive net transport by a specific term (including the dedicated sign in Eq. 1) implies that this term leads to a concentration accumulation and vice versa.

Wherever mean quantities are presented in the following, e.g. the mean flow or the mean scalar concentration, these quantities are averaged along the y-direction (marked by angled brackets), and over 3 h of simulated time (marked by an overbar). The data analysis starts 0.5 h after the first scalar emission, once a quasi-stationary state is reached for the scalar concentration.

3 Results and Discussion

Our goal is to improve the understanding of scalar transport mechanisms in the lee of forests, aiming to provide recommendations for the design and interpretation of micrometeorological measurements in fragmented forested landscapes. As a first step, well-known flow characteristics downstream of a forest-clearing transition are briefly revisited.

3.1 Flow Properties in the Lee of a Forest

Figure 3 shows $x-z$ slices of the normalized mean streamwise and vertical velocity components, $\overline{\langle u \rangle}/u_{\text{ref}}$ (a) and $\overline{\langle w \rangle}/u_{\text{ref}}$ (b), respectively, for both sparse- and dense-canopy scenarios (simulations LAI2 and LAI8). Dashed black lines bound the forest volume.

For both *LAI* values, the mean flow downstream of the forest re-attaches to the clearing surface (Fig. 3a), in the course of which the forest-typical inflected wind profile (not shown, see e.g. Finnigan 2000; Belcher et al. 2003; Queck et al. 2015) gradually adjusts to a logarithmic rough-wall wind profile. The re-attachment is consistent with the widespread negative
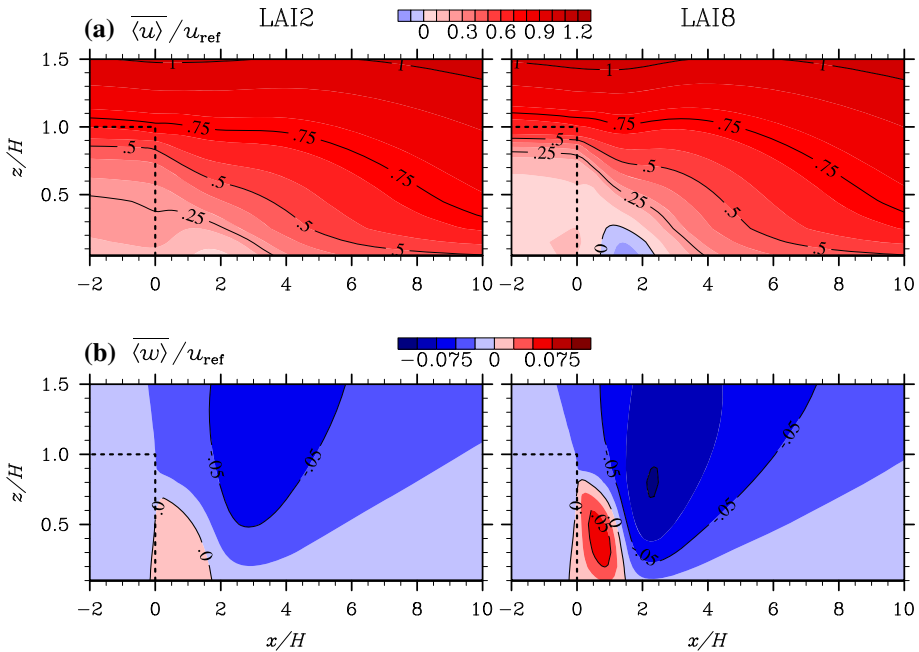
Fig. 3 Streamwise vertical slices of: mean streamwise and vertical velocity components, **a** $\overline{\langle u \rangle}$ and **b** $\overline{\langle w \rangle}$, respectively, from simulations LAI2 (*left*) and LAI8 (*right*). The mean corresponds to a spatial average in the edge-parallel direction and a 3-h time average, denoted by angled brackets and overbar, respectively. Reference velocity u_{ref} used for normalization is taken at the reference position (x_{ref}, z_{ref}) above the clearing. The rear part of the forest is shown, with the edge at $x/H = 0$ marked by the *dashed black lines*, followed by a part of the clearing

vertical velocity (Fig. 3b, dark-blue area) above the clearing. The general behaviour of the mean flow agrees well with the results of Cassiani et al. (2008) (c.f. their Figs. 6 and 9), who successfully validated their LES results against observations from various field experiments with different tree species.

Comparing cases LAI2 and LAI8 in our Fig. 3 indicates differences in the flow fields. A streamwise flow reversal is present in the lee of the dense forest (Fig. 3a), coinciding with the small region of positive $\overline{\langle w \rangle}/u_{ref}$ (Fig. 3b, red contours). The flow reversal is a result of an adverse pressure gradient, set up over a distance of a few H downstream of the edge, acting against the streamwise flow, forcing it to separate from the surface and to recirculate (Cassiani et al. 2008; Markfort et al. 2014). Such lee recirculations at the outflow edge of forests have been previously detected not only in LES (Yang et al. 2006; Cassiani et al. 2008) and RANS (Wilson and Flesch 1999) studies, but also in wind-tunnel (Markfort et al. 2014) and field experiments (Bergen 1975; Flesch and Wilson 1999; Detto et al. 2008). We found lee recirculations for $LAI \geq 3$ (see Table 2), providing a good match with results of Cassiani et al. (2008). The maximum strength of the reversed flow, $\overline{\langle u \rangle}|_{min}$,—normalized here with U_H ($=\overline{\langle u \rangle}(z = H)$ at the x-position of $\overline{\langle u \rangle}|_{min}$) in analogy to available data at a tower location— increases with LAI, as expected. The streamwise extent Δx_r of the recirculation region slightly increases with LAI, while the wind speed has no significant impact on $\overline{\langle u \rangle}|_{min}/U_H$ and Δx_r. Hence, the formation and the properties of a lee recirculation appear to depend mainly on forest morphology.

Table 2 Occurrence of lee recirculations in the mean streamwise flow for simulations LAI[1-8] and UREF[1-7]

LES run	$\overline{\langle u \rangle}|_{\min}/U_H$	$\Delta x_r\ (H)$	LES run	$\overline{\langle u \rangle}|_{\min}/U_H$	$\Delta x_r\ (H)$
LAI1	–	–	UREF1	−0.075	1.0
LAI2	–	–	UREF2	−0.077	1.0
LAI3	−0.006	0.3	UREF3	−0.078	1.0
LAI4	−0.075	1.0	UREF5	−0.077	1.0
LAI5	−0.125	1.2	UREF6	−0.076	1.0
LAI6	−0.159	1.4	UREF7	−0.073	1.0
LAI7	−0.186	1.5			
LAI8	−0.211	1.5			

The respective maximal reversed u-velocity component ($\overline{\langle u \rangle}|_{\min}$) is listed, as well as the maximum streamwise extent Δx_r of the recirculation region. The former is normalized with U_H, being $\overline{\langle u \rangle}(z = H)$ at the x-position of $\overline{\langle u \rangle}|_{\min}$
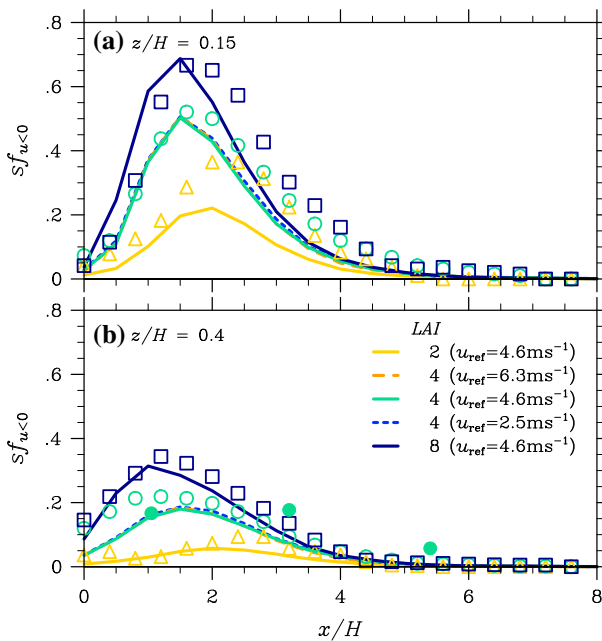

Fig. 4 Sample fraction $sf_{u<0}$ of the relative occurrence of BFS-flow events as a function of x/H, at heights **a** $z/H = 0.15$ and **b** $z/H = 0.4$: data for the present LES study (*lines*), the Cassiani et al. (2008) LES (*open symbols*) and the Flesch and Wilson (1999) field experiment (*solid symbols*)

As mentioned in Sect. 1, flow recirculations are typical for BFS flows and have an intermittent nature, both in time and along the forest edge. Cassiani et al. (2008) found the relative occurrence of recirculation events (BFS-flow events) to depend on *LAI*. Following Cassiani et al. (2008), we analyzed the sample fraction $sf_{u<0}$ of BFS-flow events as presented in Fig. 4 (solid/dashed lines; symbols reflect data of other studies), with $sf_{u<0}$ being the number of measured samples with negative u divided by the total number of samples. Samples were taken at each timestep in a 3-h time interval, and at each grid point along the y-direction for
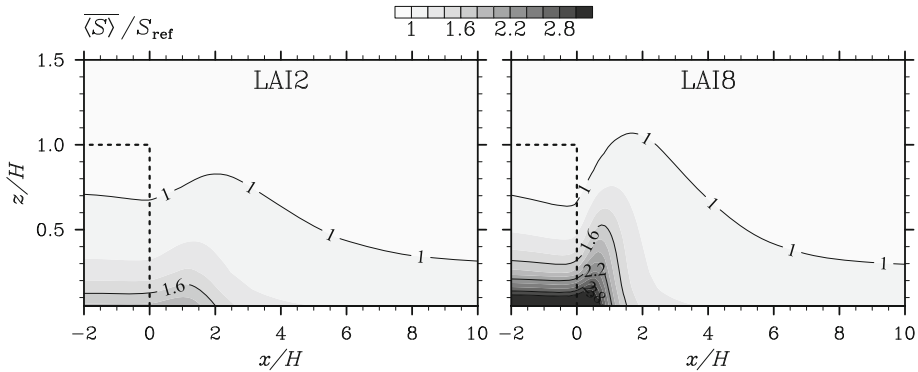
Fig. 5 Streamwise vertical slices of mean concentration $\overline{\langle S \rangle}$, for simulations LAI2 and LAI8. Reference concentration S_{ref}, used for normalization, is taken at reference position $(x_{\text{ref}}, z_{\text{ref}})$ above the clearing. The forest volume is bounded by the *dashed black lines*

selected x–z positions, resulting in a total of $\mathcal{O}(10^5)$ samples for each (x, z) coordinate. At both heights, $z/H = 0.15$ (Fig. 4a) and $z/H = 0.4$ (b), and for all presented *LAI* and wind-speed values, $sf_{u<0}$ forms a peak somewhere within $1 < x/H < 2$—the region where the reversed flow is visible in $\overline{\langle u \rangle}(x, z)$ (not shown for all *LAI* values). Downstream of the peak, $sf_{u<0}$ decreases towards zero. Superposed solid and dashed lines for simulations LAI4 reveal that the wind speed has no effect on the relative occurrence of BFS-flow events. In contrast, the number of BFS-flow events significantly increases with *LAI*, as reported by Cassiani et al. (2008). We found this increase to converge for $LAI \geq 6$ (not shown here for reasons of clarity). Our $sf_{u<0}$ data are in good agreement with results of the Cassiani et al. (2008) LES (open symbols) and the Flesch and Wilson (1999) field experiment (solid symbols), giving confidence to our results. Only for the case LAI2 at $z/H = 0.15$ (Fig. 4a, yellow line), can large deviations to the $sf_{u<0}$ values of Cassiani et al. (2008) (triangles) be detected, and may be due to the different vertical leaf distributions in the respective simulations, having a more pronounced effect near the surface and for sparser forests. Overall, $sf_{u<0}$ could be a useful quantity for the dynamical characterization of the flow in the forest lee, applied again in Sect. 3.4.

3.2 Scalar Distribution in the Lee of Forests and the Responsible Transport Mechanisms

As known from previous studies, concentrations can be locally enhanced in regions with flow separation and recirculation, whether in the lee of a hill (Katul et al. 2006; Poggi and Katul 2007; Ross 2011; Ross and Baker 2013) or even deep inside a forest canopy (Sogachev et al. 2008; Kanani-Sühring and Raasch 2015). Figure 5 shows x–z slices of the mean scalar concentration $\overline{\langle S \rangle}$ for simulations LAI2 and LAI8, normalized with the reference concentration S_{ref}, equalling the mean concentration above the clearing surface at $(x_{\text{ref}} = 33H, z_{\text{ref}} = 0.35H)$.

For the most part, near-surface concentrations are lower above the clearing than on the forest patch, owing to greater advection and turbulent mixing above the clearing. The only exception is the lee region, where the scalar accumulates with local overshoots of $\overline{\langle S \rangle}$ over S_{ref} of 20% (LAI2) and 100% (LAI8) at z_{ref}. Numerical simulations by Ross (2011) and by Ross and Baker (2013) of the flow across fully forested hills revealed a similar local
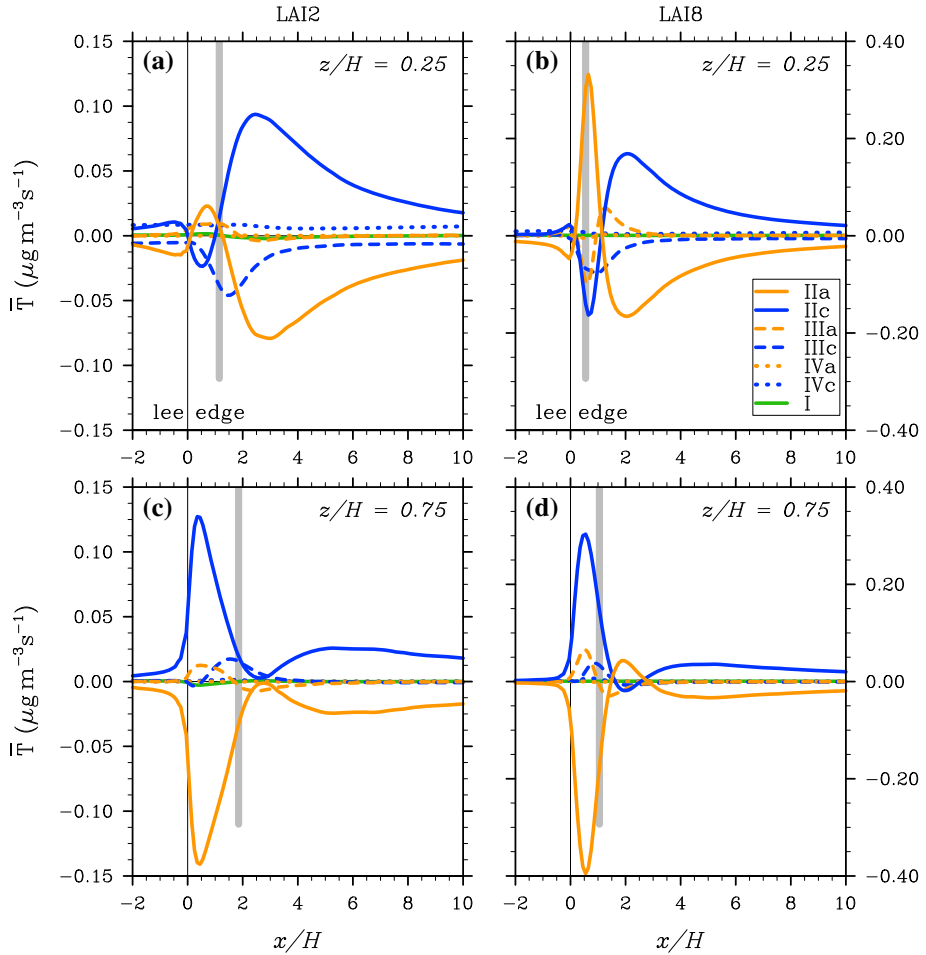
Fig. 6 Scalar balance terms $\overline{T} \in \{I, II, III, IV\}$, time averaged over 3 h of simulated time, **a**, **b** at $z/H = 0.25$ and **c**, **d** at $z/H = 0.75$, for simulations LAI2 and LAI8. Term I: temporal change of S; terms II, III, IV: net transport of S by the mean flow, by resolved scale turbulence and by subgrid-scale turbulence in the streamwise (II–IVa) and vertical (II–IVc) direction. The leeward edge is at $x/H = 0$. For comparison, the location of the scalar concentration peak at the respective height and *LAI* value is marked by the *vertical grey line*

scalar accumulation on the lee-side of the hill, with similar peak strengths as detected in our simulations. For the case of only partially forested hills, results of Ross and Baker (2013) further indicated a dependency of the peak strength on the location of the forest patch with respect to the hill summit.

To identify responsible mechanisms for the accumulation, we analyzed the terms of the scalar balance equation (Eq. 1). Figure 6 shows the streamwise evolution of each term, $\overline{T} \in \{\overline{I}, \overline{II}, \overline{III}, \overline{IV}\}$ for simulations LAI2 (a, c) and LAI8 (b, d), at the heights $z/H = 0.25$ (a, b) and $z/H = 0.75$ (c, d) as representatives for the mechanisms in the lower and the upper half of the lee region. Each curve shows the time-averaged net transport of S by one of the transport terms $\overline{T}$ at the given (x, z) position; positive values describe a concentration enhancement by that term and vice versa.

Overall, the streamwise evolution of a specific term is similar for simulations LAI2 and LAI8 at a given height, except for the generally smaller values for LAI2 (note the different ordinates). This is because the disturbance of the flow, and hence of the scalar transport, is less pronounced for a sparse forest. Except for the subgrid-scale terms (IVa, c), which are more or less constant or small compared to the other terms, all terms are largest within $3H$ distance from the leeward edge. This is where the largest impact of the flow can be found, e.g. with the occurrence of intermittent BFS-flow events (see Sect. 3.1). Further downstream, where the flow adjusts to a horizontal and homogeneous flow [until it is affected by the windward forest edge (c.f. Kanani-Sühring and Raasch 2015, Fig. 5)], the balance terms accordingly decrease towards zero (not shown); terms IIIc and IVc form an exception, as they take over the vertical mixing of the surface-emitted scalar. The subgrid-scale vertical turbulent net transport (IVc) is not further treated, since with its rather small streamwise-constant values, it exhibits no direct effect on the local scalar accumulation. Thus, when referring to turbulence or turbulent net transport in the following, we refer to the resolved-scale part of turbulence.

First, the near-surface transport is discussed by means of Fig. 6a, b. For case LAI8 (b), with a mean flow reversal in the lee region (see Fig. 3a), the scalar peak (grey line) coincides with the positive peak of term IIa; i.e., the scalar peak falls in the region of strongest streamwise mean-flow convergence as expected. Consequently, the mean streamwise net transport (solid orange) leads to an accumulation of the scalar, while the mean vertical transport (solid blue) as well as the streamwise and vertical turbulent transports (dashed orange and blue) are responsible for the depletion of the scalar. The turbulent net transport is of the same order of magnitude as that of the vertical mean flow, indicating that all transport mechanisms are equally important here.

In the case without lee recirculation, e.g. as for the LAI2 simulation (see Fig. 3a), the individual transport mechanisms in the scalar peak region (Fig. 6a) interact differently compared to those in simulation LAI8 (Fig. 6b). The scalar peak (grey line) in simulation LAI2 is not found at the position of the IIa peak, but rather at the intersection of terms IIa,c and IIIa; i.e., these three terms are in equal parts responsible for the scalar accumulation, and not only term IIa as in simulation LAI8. The scalar depletion in simulation LAI2 is mainly achieved by the turbulent vertical net transport (dashed blue).

As expected, transport terms at the upper level (Fig. 6c, d) show a different behaviour compared to those at $z/H = 0.25$. At $z/H = 0.75$, the scalar enhancement in the scalar-peak region (grey line) is taken over by vertical net transports with the mean and the turbulent flow (solid and dashed blue). The two transport terms are equally important for the scalar accumulation in the lee of the sparse forest; for the dense forest, the vertical net transport by the mean flow (IIc) makes a 3-fold higher contribution than the turbulent counterpart (IIIc) in the grey-shaded region, attributed to the presence of the flow reversal. The streamwise net transport by turbulence (IIIa) exposes an inflection point exactly at the scalar peak location, again owing to the flow reversal; this indicates that term IIIa enhances the concentrations upstream and decreases them downstream of the scalar peak. For both *LAI* values, the scalar depletion at this height results mainly from the divergence of the streamwise transport by the mean flow (IIa).

This analysis has demonstrated that advective transport processes are as important as the turbulent transport in the lee of forests. Similar conclusions were drawn by Ross and Harman (2015) for scalar transport in the lee of hills, and for different source configurations of the scalar. The large values of the term IIa (Fig. 6c, d) imply that the streamwise advection is not negligible for the scalar transport here; this must be considered for the interpretation of eddy-covariance measurements (Foken 2008), which disregard flux contributions from advective transports.
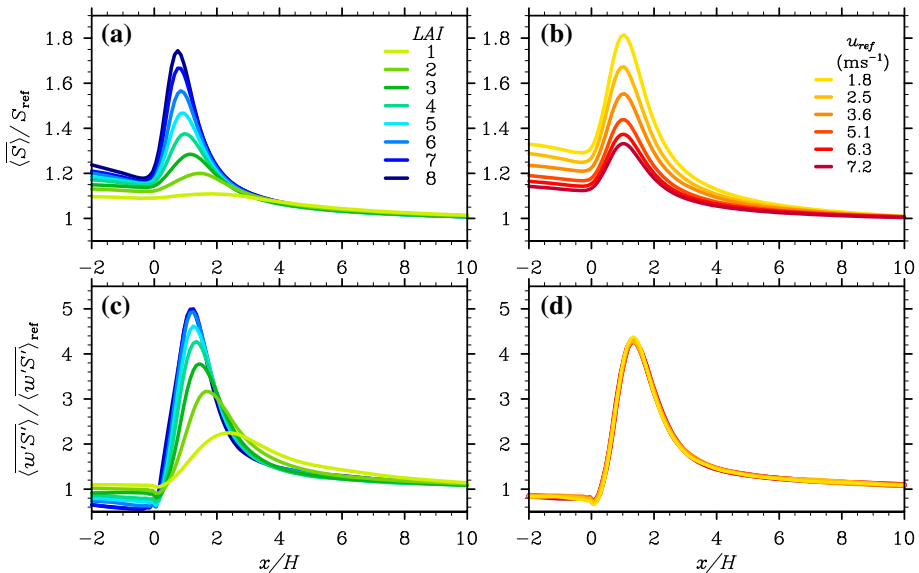
Fig. 7 Streamwise evolution of the mean **a**, **b** concentrations and **c**, **d** fluxes, normalized with their reference values S_{ref} and $\overline{\langle w'S'\rangle}_{ref}$, respectively. $\overline{\langle w'S'\rangle}_{ref}$ is taken from the same location as S_{ref}. All simulated **a**, **c** *LAI* and **b**, **d** UREF cases are presented at $z/H = 0.4$

3.3 Behaviour of Concentration and Flux Distributions under Different Atmospheric, Plant-Physiological and Source Conditions

Section 3.2 has identified physical mechanisms that lead to the local scalar accumulation. It is further examined below to what extent the accumulation depends on *LAI*, wind speed and scalar-source distribution (see Sect. 2). Figure 7 presents the streamwise distribution of the normalized mean scalar concentration $\overline{\langle S\rangle}/S_{ref}$ (a, b) and the normalized scalar flux $\overline{\langle w'S'\rangle}/\overline{\langle w'S'\rangle}_{ref}$ (c, d) at $z/H = 0.4$ for different *LAI* (a, c) and u_{ref} (b, d) values. Reference values are taken from the same height level at reference position x_{ref}.

The peak location is only slightly affected by *LAI* or wind speed, with deviations of less than $1H$. This is much different to that found by Kanani-Sühring and Raasch (2015) for the behaviour of the scalar accumulation on the forest patch; there, the distance between windward forest edge and scalar peak location was largely dependent on *LAI* ($\approx 10H$ variation between simulations LAI1 and LAI8), due to the proportionality between *LAI* and the volume drag forces; in the forest lee, the direct canopy drag is absent, consequently, the peak position is nearly invariant of *LAI*.

In contrast, the concentration peak values show large differences among the *LAI* and UREF cases. The peak concentration for case LAI8 overshoots S_{ref} by 75%; for case LAI2, it is a 20% overshoot, almost a factor of four difference. A factor of two lies between the percentage overshoots of cases UREF1 and UREF7. For all cases, concentrations are adjusted to $1.05\,S_{ref}$ (5% tolerance) downstream of $x/H \approx 6$. In general, the largest near-edge concentrations must be expected in the lee of dense forests under weak-wind conditions.

Also the scalar fluxes strongly depend on *LAI* (Fig. 7c), with peak values ranging roughly from $2\,\overline{\langle w'S'\rangle}_{ref}$ for simulation LAI1 to $5\,\overline{\langle w'S'\rangle}_{ref}$ for simulation LAI8. Peak values converge for $LAI \geq 6$, suggesting that an upper limit is reached for the local flux enhancement. The
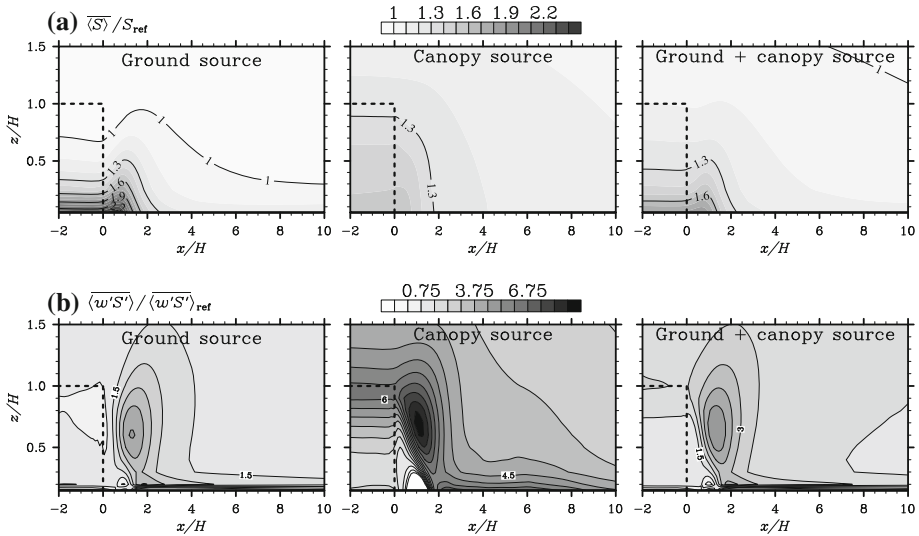
Fig. 8 Streamwise vertical slices of the normalized **a** mean concentration $\overline{\langle S \rangle}/S_{ref}$ and **b** mean scalar flux $\overline{\langle w'S' \rangle}/\langle w'S' \rangle_{ref}$, for simulation LAI4 with three different source distributions. Reference values for normalization are taken at the reference position (x_{ref}, z_{ref}) above the clearing. The forest volume is bounded by the *dashed black lines*

wind speed appears to have almost no effect on the flux distribution (Fig. 7d), although scalar concentrations do show a wind-speed dependence. The same was detected and discussed in detail by Kanani-Sühring and Raasch (2015) for the fluxes above the forest patch, who attributed this invariance to the fact that larger w fluctuations, appearing under higher wind speeds due to the larger shear, are compensated by relatively small S fluctuations, and vice versa.

A modification of the source distribution affects both concentration and flux distribution, as visualized in Fig. 8 by vertical slices of the normalized mean concentration (a) and flux (b). The total turbulent scalar flux is visualized here, i.e. the sum of resolved-scale and subgrid-scale fluxes though, except for the near-surface levels, the contribution of the subgrid scales is negligible. Switching from ground to canopy source produces an increase in background concentration, owing to the elevated sources that allow increased mixing of the scalar between the canopy and the atmosphere above. Further, no local scalar accumulation exists in the case of a canopy source; instead, concentrations quickly decrease with distance to the leeward edge, as scalar-poor air descends into the clearing. Despite the rather homogeneous concentration field in the canopy-source simulation, the flux field exposes a pronounced peak in the immediate lee, with even higher values than observed for the ground-source case. In the mixed-source set-up, isolines show a closer similarity to the ground-source case, while the magnitude of the values is somehow affected by the canopy source. Regardless of the sources, enhanced scalar fluxes are observed in the lee region.

Overall, the appearance of locally enhanced scalar concentrations and fluxes, as well as their dependence on forest morphology, scalar source distribution and wind speed (and on landscape topography as reported e.g. by Ross 2011; Ross and Baker 2013), highlight that in situ concentration and flux measurements should be interpreted with special care.
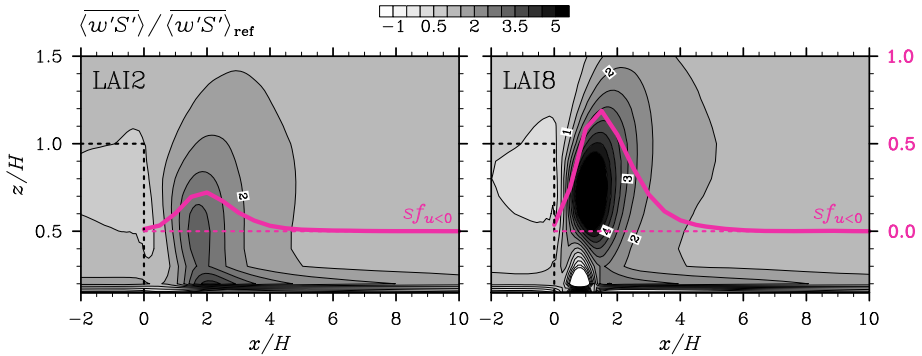
Fig. 9 x–z slices of the mean scalar flux $\overline{\langle w'S' \rangle}$, normalized with $\overline{\langle w'S' \rangle}_{\text{ref}}$, for simulations LAI2 and LAI8. For comparison, the measure for the relative occurrence of BFS-flow events, $sf_{u<0}$ at $z/H = 0.15$ (see Fig. 4), is illustrated by the *red curves* with corresponding labels on the right-hand-side ordinate

3.4 Interpretation of Micrometeorological Measurements in the Lee of Forests

Our results question the spatial representativity of in situ micrometeorological measurements above forest clearings. As discussed for Fig. 8, scalar fluxes (and concentrations) are locally enhanced, (almost) independent of the source configuration. Figure 9 presents two additional x–z slices of the mean normalized scalar flux for simulations LAI2 and LAI8 (ground source). As discussed by means of Fig. 7, peak fluxes are much larger for simulation LAI8 than for simulation LAI2. Near-surface fluxes ($0.1 < z/H < 0.2$) are adjusted to their respective equilibrium values, with 5% tolerance ($1.05 \overline{\langle w'S' \rangle}_{\text{ref}}$), at about $25H$ downstream of the leeward forest edge (not shown), almost independent of *LAI* and wind speed. At larger heights, a distance of at least $15H$ is required between the leeward edge and the measuring position to ensure the measurement of adjusted rather than edge-disturbed fluxes. The region of extreme flux enhancement – bounded by the 2-isoline that equals a 100% overshoot over the equilibrium value $\overline{\langle w'S' \rangle}_{\text{ref}}$ – extends to $x/H \approx 3$ in both cases, and reaches up to $z/H \approx 1.5$ for dense forests. Thus, if experimental sites are located within the enhanced-flux region, large deviations must be expected between the measured flux and the clearing-representative flux, particularly for dense forests; i.e., these measurements might not be suitable for a reliable estimate of a representative clearing flux. According to Figs. 8 and 9, this seems to be the case for ground- or canopy-emitted scalars; however, this conclusion is made here for passive (weakly reactive) scalars, with further examination required for (re)active scalars.

By all means, measurements in the region of reversing flow should be avoided, as this is indicative of the region where the influence of the forest is strongest. The sample fraction $sf_{u<0}$ (see Sect. 3.1) marks this region (red curves in Fig. 9), where the peak of $sf_{u<0}$ coincides with the flux peak. Further downstream, $sf_{u<0}$ quickly approaches zero, while $\overline{\langle w'S' \rangle}$ adjusts to its equilibrium value. Larger $sf_{u<0}$ values generally indicate a larger relative flux enhancement, and Fig. 10 illustrates this behaviour by means of a scatter plot of $sf_{u<0}$ ($x/H, z/H = 0.15$) against the maximal flux value along z at each x-position divided by its equilibrium value.

To conclude, $sf_{u<0}$ can be used as an indicator for the relative flux enhancement—and $sf_{u<0}$ is easily retrieved from high-frequency sonic anemometer data—but an absence of flow reversals does not necessarily imply that there is no flux enhancement. Also, forests are often three-dimensionally heterogeneous in nature, and edges are usually not straight and homogeneous, so that it might be difficult to detect flow reversals at complex sites. However,
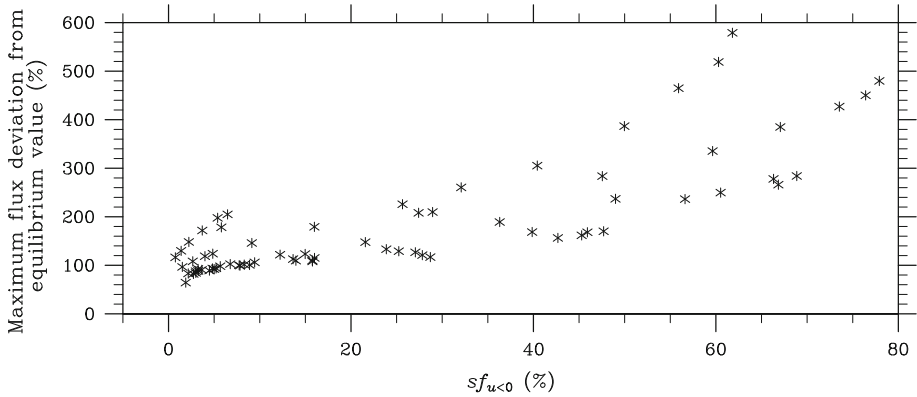
Fig. 10 $sf_{u<0}(x/H, z/H = 0.15)$ plotted against the maximal flux value along z at each x-position divided by its equilibrium value. Data points are taken from $0 < x/H < 5$, and for the various LAI values

there have been reports of flow reversals in previous field experiments (e.g. Flesch and Wilson 1999; Detto et al. 2008; Queck et al. 2015), so this is still an open point that needs detailed attention by means of more realistic LES. First and foremost, measurements at $x/H < 3$ should be avoided, because fluxes are overestimated by more than 100% in this region, as compared to further downstream, where the overestimation quickly decreases to $\approx 10\%$.

4 Summary

By means of LES, we examined the scalar transport in neutral flows across idealized forest-clearing transitions in flat terrain. The goal was to enable a better planning and interpretation of in situ micrometeorological measurements. This is a follow-up study to that of Kanani-Sühring and Raasch (2015), where locally enhanced scalar concentrations and fluxes were found above a forest patch downstream of a clearing-forest transition.

In the present study, we found locally enhanced scalar concentrations and scalar fluxes in the forest lee, for a wide range of *LAI* values and wind speeds. Similar accumulations of surface-emitted scalars were previously observed in the lee of fully and partially forested hills (e.g. Katul et al. 2006; Ross and Baker 2013; Ross and Harman 2015). An analysis of the scalar balance terms revealed that the relative importance of individual transport terms strongly depends on *LAI*. For large *LAI* values, the convergence of the mean streamwise transport of scalar is solely responsible for the local scalar enhancement, while for sparser forests, mean and turbulent transports are equally responsible. This is attributed to the strength of the recirculating flow in the lee of forests [as in backward-facing step flow (e.g. Armaly et al. 1983; Kostas et al. 2002; Markfort et al. 2014)], having an intermittent nature. By means of LES (Cassiani et al. 2008) and field experiments (Flesch and Wilson 1999; Detto et al. 2008), the relative occurrence of flow reversals has been found to increase with forest density. The equal importance of advective and turbulent transport, as also concluded by Ross and Harman (2015) for a forested-hill scenario, needs to be considered for the interpretation of eddy-covariance measurements (Foken 2008), which disregard flux contributions from advective transport.

We found peak concentrations to increase with increasing *LAI* and with decreasing wind speed, conforming to the results above the forest patch (Kanani-Sühring and Raasch 2015).

However, peak positions in the lee were nearly unaffected by wind speed and *LAI*, in contrast to the strong dependency on *LAI* above the forest patch. Scalar fluxes in the forest lee likewise increase with forest density, while they are invariant with wind speed. The locally enhanced fluxes were found for ground- and canopy-emitted scalars. Overall, the peaks of scalar concentration and scalar flux are of the same order of magnitude as detected in LES by Ross (2011), Ross and Baker (2013), Ross and Harman (2015) in the lee of forested hills, where similar physical mechanisms lead to an accumulation of the scalar.

This local enhancement adds complexity to the interpretation of in situ micrometeorological measurements. Based on the flux fields, we suggest a minimum distance of $3H$ to be placed between the measuring equipment and the lee edge of a forest. We further found that the relative frequency of intermittent flow reversals—this information can be extracted from sonic anemometer data—is related to the magnitude of the flux enhancement.

It should be noted that our results hold for neutral conditions with low to moderate wind speeds, for the simulated forest-clearing configuration, and for different scalar-source configurations. To what extent the above mentioned relations and recommendations might change under other meteorological conditions (e.g. stable or unstable stratification), or more heterogeneous landscape or forest configurations (see e.g. Dupont et al. 2011; Schlegel et al. 2014) is the subject for further study.

References

Armaly BF, Dursts F, Pereira JCF, Schönung B (1983) Experimental and theoretical investigation of backward-facing step flow. J Fluid Mech 127:473–496

Belcher SE, Jerram N, Hunt JCR (2003) Adjustment of a turbulent boundary layer to a canopy of roughness elements. J Fluid Mech 488:369–398

Belcher SE, Harman IN, Finnigan JJ (2012) The wind in the willows: flows in forest canopies in complex terrain. Annu Rev Fluid Mech 44:479–504

Bergen JD (1975) Air movement in a forest clearing as indicated by smoke drift. Agric Meteorol 15:165–179

Cai XM, Barlow JF, Belcher SE (2008) Dispersion and transfer of passive scalars in and above street canyons—large-eddy simulations. Atmos Environ 42:5885–5895

Cassiani M, Katul GG, Albertson JD (2008) The effects of canopy leaf area index on airflow across forest edges: large-eddy simulation and analytical results. Boundary-Layer Meteorol 126:433–460

Chan TL, Dong G, Leung CW, Cheung CS, Hung WT (2002) Validation of a two-dimensional pollutant dispersion model in an isolated street canyon. Atmos Environ 36:861–872

Detto M, Katull GG, Siqueira M, Juang JY, Stoy P (2008) The structure of turbulence near a tall forest edge: the backward-facing step flow analogy revisited. Ecol Appl 18:1420–1435

Dupont S, Brunet Y (2008) Edge flow and canopy structure: a large-eddy simulation study. Boundary-Layer Meteorol 126:51–71

Dupont S, Bonnefond JM, Irvine MR, Lamaud E, Brunet Y (2011) Long-distance edge effects in a pine forest with a deep and sparse trunk space: in situ and numerical experiments. Agric For Meteorol 151:328–344

Finnigan JJ (2000) Turbulence in plant canopies. Annu Rev Fluid Mech 32:519–571

Finnigan JJ, Belcher SE (2004) Flow over a hill covered with a plant canopy. Q J R Meteorol Soc 130:1–29

Flesch TK, Wilson JD (1999) Wind and remnant tree sway in forest cutblocks. I. Measured winds in experimental cutblocks. Agric For Meteorol 93:229–242

Foken T (2008) Micrometeorology. Springer, Berlin 306 pp

Fontan S, Katul GG, Poggi D, Manes C, Ridol L (2013) Flume experiments on turbulent flows across gaps of permeable and impermeable boundaries. Boundary-Layer Meteorol 147:21–39

Frank C, Ruck B (2008) Numerical study of the airflow over forest clearings. Forestry 81:259–277

Kanani-Sühring F, Raasch S (2015) Spatial variability of scalar concentrations and fluxes downstream of a clearing-to-forest transition: an LES study. Boundary-Layer Meteorol 155:1–27

Katul GG, Finnigan JJ, Poggi D, Leuning R, Belcher SE (2006) The influence of hilly terrain on canopy-atmosphere carbon dioxide exchange. Boundary-Layer Meteorol 118:189–216

Klaassen W, Van Breugel PB, Moors EJ, Nieveen JP (2002) Increased heat fluxes near a forest edge. Theor Appl Climatol 72:231–243

Kostas J, Soria J, Chong MS (2002) Particle image velocimetry measurements of a backward-facing step flow. Exp Fluids 33:838–853

Letzel MO, Krane M, Raasch S (2008) High resolution urban large-eddy simulation studies from street canyon to neighbourhood scale. Atmos Environ 42:8770–8784

Letzel MO, Helmke C, Ng E, An X, Lai A, Raasch S (2012) LES case study on pedestrian level ventilation in two neighbourhoods in Hong Kong. Meteorol Z 21:575–589

Markfort CD, Porté-Agel F, Stefan HG (2014) Canopy-wake dynamics and wind sheltering effects on Earth surface fluxes. Environ Fluid Mech 14:663–697

Maronga B, Gryschka M, Heinze R, Hoffmann F, Kanani-Sühring F, Keck M, Ketelsen K, Letzel MO, Sühring M, Raasch S (2015) The parallelized large-eddy simulation model (PALM) version 4.0 for atmospheric and oceanic flows: model formulation, recent developments, and future perspectives. Geosci Model Dev 8:2515–2551

Miller DR, Lin JD, Lu ZN (1991) Air flow across an alpine forest clearing: a model and field measurements. Agric For Meteorol 56:209–225

Poggi D, Katul GG (2007) Turbulent flows on forested hilly region terrain: the recirculation. Q J R Meteorol Soc 133:1027–1039

Queck R, Bernhofer C, Bienert A, Eipper T, Goldberg V, Harmansa S, Hildebrand V, Maas HG, Schlegel F, Stiller J (2015) TurbEFA: an interdisciplinary effort to investigate the turbulent flow across a forest clearing. Meteorol Z 23:637–659

Raasch S, Schröter M (2001) PALM—a large-eddy simulation model performing on massively parallel computers. Meteorol Z 10:363–372

Raupach MR, Weng WS, Carruthers DJ, Hunt JCR (1992) Temperature and humidity fields and fluxes over low hills. Q J R Meteorol Soc 118:191–225

Ross AN (2008) Large-eddy simulations of flow over forested ridges. Boundary-Layer Meteorol 128:59–76

Ross AN (2011) Scalar transport over forested hills. Boundary-Layer Meteorol 141:179–199

Ross AN, Baker TP (2013) Flow over partially forested ridges. Boundary-Layer Meteorol 146:375–392

Ross AN, Harman IN (2015) The impact of source distribution on scalar transport over forested hills. Boundary-Layer Meteorol 156:211–230

Schlegel F, Stiller J, Bienert A, Hg Maas, Queck R, Bernhofer C (2014) Large-eddy simulation study of the effects on flow of a heterogeneous forest at sub-tree resolution. Boundary-Layer Meteorol 154:27–56

Sogachev A, Leclerc MY, Zhang G, Rannik Ü, Vesala T (2008) CO_2 fluxes near a forest edge: a numerical study. Ecol Appl 18:1454–1469

Wilson JD, Flesch TK (1999) Wind and remnant tree sway in forest cutblocks. III. A windflow model to diagnose spatial variation. Agric For Meteorol 93:259–282

Yang B, Raupach MR, Shaw RH, Paw UKT, Morse AP (2006) Large-eddy simulation of turbulent flow across a forest edge. Part I: flow statistics. Boundary-Layer Meteorol 120:377–412